Selective Proton-Mediated Transport by Electrogenic K+-Binding Macrocycles

Yu-Hao Li, Shao-Ping Zheng, Dawei Wang, Mihail Barboiu

chemistry

MDPI

Article

Selective Proton-Mediated Transport by Electrogenic K^+-Binding Macrocycles

Yu-Hao Li [1], Shao-Ping Zheng [1], Dawei Wang [1] and Mihail Barboiu [1,2,*]

[1] Lehn Institute of Functional Materials, School of Chemistry, Sun Yat-Sen University, Guangzhou 510275, China; yuhaoli.mat@gmail.com (Y.-H.L.); zhshaop@126.com (S.-P.Z.); wdawei@mail.sysu.edu.cn (D.W.)

[2] Adaptive Supramolecular Nanosystems Group, Institut Européen des Membranes, University of Montpellier ENSCM-UM-CNRS UMR-5635, Place E. Bataillon, CC 047, F-34095 Montpellier, France

* Correspondence: mihail-dumitru.barboiu@umontpellier.fr

Received: 13 December 2019; Accepted: 16 January 2020; Published: 20 January 2020

Abstract: Synthetic K^+-binding macrocycles have potential as therapeutic agents for diseases associated with KcsA K^+ channel dysfunction. We recently discovered that artificial self-assembled *n*-alkyl-benzoureido-15-crown-5-ether form selective ion-channels for K^+ cations, which are highly preferred to Na^+ cations. Here, we describe an impressive selective activation of the K^+ transport via electrogenic macrocycles, stimulated by the addition of the carbonyl cyanide-4-(trifluoromethoxy) phenylhydrazone (FCCP) proton carrier. The transport performances show that both the position of branching or the size of appended alkyl arms favor high transport activity and selectivity S_{K^+/Na^+} up to 48.8, one of the best values reported up to now. Our study demonstrates that high K^+/Na^+ selectivity obtained with natural KcsA K^+ channels is achievable using simpler artificial macrocycles displaying constitutional functions.

Keywords: ion-channels; crown-ethers; bilayer membranes; self-assembly; supramolecular chemistry

1. Introduction

Facilitated transmembrane transport by molecular carriers that selectively recognize and transport ionic species is an important and complex physiological process [1]. Nature has evolved millions of years to generate highly selective cation carriers, for which the transport mechanisms are controlled via a membrane potential (i.e., electrogenic valinomycin) or pH gradient (i.e., neutral monensin) [2]. Most of the previously reported artificial systems cannot achieve this type of stable potential, due to their poor selectivity. Macrocyclic crown-ethers have already proven to be efficient cation channels [2,3]. Whether these macrocycles are covalently connected [3–7] or self-assembled via H-bonding [8–19], they form ion-channels, performing effective transport of ions across lipid bilayers. The structural variation between closely related synthetic carriers or channels could lead to a huge difference in activities [8–14].

Artificial ion-channels presenting high K^+/Na^+ selectivity are rare. We unexpectedly discovered that benzo-15-crown-5-ethers are showing far superior selectivity for K^+ cation when compared with benzo-18-crown-6 congeners [15–19]. So far, research efforts have mainly focused on the electrogenic polarization across the membrane, related to a net transfer of charge via neutral alkyl-benzoureido-15-crown-5-ether channels [15]. Moreover, we also demonstrated that cholesteric or squalene moieties appended to cation binding benzo-15-crown-5-ether show the most efficient transport among similar structures to a certain extent [16]. Under the same conditions, squalene-benzoamido-15-crown-5-ether has the highest selectivity for K^+ over Na^+, $S_{K+/Na+}$ = 58.3, [17] while hexylbenzo-ureido-15-crown-5-ether has lower $S_{K+/Na+}$ = 17 [15].

We know from previous studies [20–24] that the transport activity has an optimal relationship with lipophilicity of carriers, while the disposition of the alkyl groups on the carrier backbone proved to be important too. The self-assembly behaviors of the functional transporting system are directly determining the structural dynamics that control the self-organized superstructures along cation recognition and transport pathways. The transport mechanism is determined by the optimal coordination rather than classical dimensional compatibility between crown-ether and cation, and systematic changes of the structure lead to adaptive selection in cation-transport activity [25].

As far as we know the alkyl skeleton isomerism was rarely considered to be a determinant factor to influence the transport activity. The structural variability of the alkyl tails of the macrocyclic superstructures at the interface within the membrane have been not specifically studied in our previous work. Herein, we continue our exploration and we serendipitously found that simple small variations on the structure of the linear or branched octyl tails in octyl-benzoureido-15-crown-5-ethers **1**, **r2**, **s2,** and racemic **3** (Figure 1, Scheme S1) are strongly influencing the transport activities of monovalent cations. Together with this result, we confirmed another unexpected phenomenon; the carrier-induced electrogenic influx of K^+ cations is considerably boosted when coupled with proton transporter like carbonyl cyanide-4-(trifluoromethoxy) phenylhydrazone (FCCP) [25].

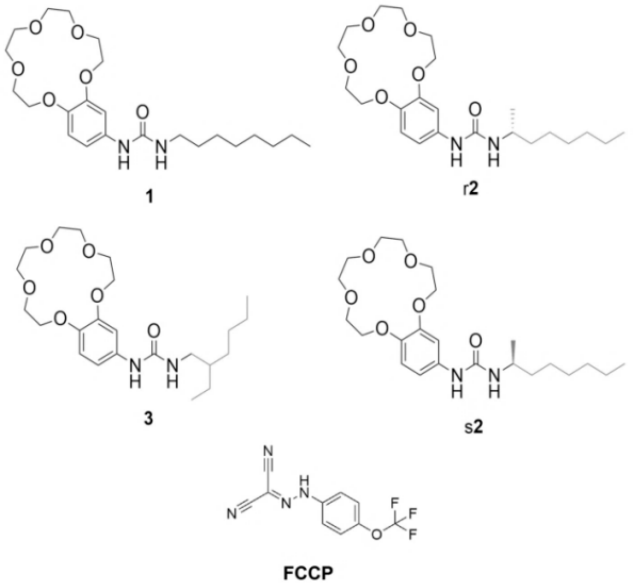

Figure 1. Crown-ether compounds **1**, **r2**, **s2**, **3** and the H^+ transporter carbonyl cyanide-4-(trifluoromethoxy)phenylhydrazone (FCCP) reported in this article.

Simultaneous addition of **1**, **r2**, **s2**, **3** and FCCP leads to the induction of K^+/H^+ antiport via the formation of an electrical potentials across the membrane. This coupling of K^+ and H^+ fluxes can proceed without a potential via non-electrogenic K^+/H^+ exchanges across the membrane. We observe an unprecedented increase in the selectivity [15,16] from $S_{K+/Na+}$ = 3.6 to 48.8 in the best case.

2. Materials and Methods

2.1. Materials

Octyl isocyanate, (*R*)-(−)-2-octyl isocyanate, (*S*)-(+)-2-octyl isocyanate, 2-ethylhexyl isocyanate, and FCCP were purchased from Sigma Aldrich, Paris, France. 8-hydroxypyrene-1,3,6-trisulfonic acid trisodium salt (HPTS) was purchased from Fluka, Paris, France. 4′-Aminobenzo-15-crown-5 was purchased from TCI Europe, Zwijndrecht, Belgium. L-*α*-Phosphatidylcholine EYPC was purchased from Avanti Polar Lipids, Alabaster, AL, USA and used as received.

2.2. Methods

^{1}H NMR spectra were recorded on an ARX 300 MHz Bruker Spectrometer (Bruker Daltonics, Billerica, MA, USA). Chemical shifts are reported as δ values (ppm) with corresponding deuterated solvent peak as an internal standard. Mass spectrometric analysis was performed in the positive ion mode using a quadrupole mass spectrometer (Micromass, Platform II spectrometer). Fluorescence spectra were recorded in Perkin Elmer LS-55 spectrometer (Perkin Elmer Inc., Waltham, MA, USA).

2.3. General Synthetic Procedure

All compounds have been synthesized as follows: 0.2 mmol 4′-aminobenzo-15-crown-5 are mixed with the corresponding 1.1 equiv. isocyanate in 10 mL of chloroform. The solution was stirred under reflux overnight. Solution was concentrated under rotary evaporator. Hexane was introduced to precipitate the product, after filtration, the filter cake was dried in the air and yields as final product, yields are around 65%.

1-(Benzo-15-crown-5-15-yl)-3-octylurea (**1**), ^{1}H NMR (DMSO-d_6, 300 MHz, 298 K) δ 8.19 (s, 1H), 7.13 (d, *J* = 2.1 Hz, 1H), 6.77 (dt, *J* = 8.6, 5.4 Hz, 2H), 6.00 (t, *J* = 5.6 Hz, 1H), 3.98 (dd, *J* = 8.6, 4.1 Hz, 4H), 3.74 (dd, *J* = 10.7, 6.0 Hz, 4H), 3.60 (s, 8H), 3.04 (dd, *J* = 12.6, 6.6 Hz, 2H), 1.40 (s, 2H), 1.26 (s, 10H), 0.86 (t, *J* = 6.6 Hz, 3H). ^{13}C NMR (75 MHz, $CDCl_3$, 298 K) δ 156.89, 149.56, 145.71, 132.33, 114.99, 114.49, 108.70, 70.89, 70.79, 70.42, 70.26, 69.61, 69.38, 68.55, 40.43, 31.81, 30.12, 29.31, 29.25, 26.93, 22.64, 14.09. ESI-MS Calcd. for $C_{23}H_{39}N_2O_6$ (M + H^+) 439.28, Found 439.38; Calcd. for $C_{23}H_{38}N_2O_6Na$ (M + Na^+) 461.55, Found 461.35. IR (cm^{-1}): 3297, 2924, 2855, 1627, 1559, 1516, 1457, 1417, 1269, 1233, 1135, 985, 937, 847, 628. HR-MS (ESI+) calcd. for $C_{23}H_{39}N_2O_6$ 439.2808 found *m*/*z* 439.2814.

(R)-(Benzo-15-crown-5-15-yl)-3-(octan-2-yl)urea (**r2**), ^{1}H NMR (300 MHz, 298 K, DMSO-d_6) δ 8.08 (s, 1H), 7.14 (d, *J* = 2.3 Hz, 1H), 6.81 (d, *J* = 8.7 Hz, 1H), 6.73 (dd, *J* = 8.6, 2.3 Hz, 1H), 5.83 (d, *J* = 8.1 Hz, 1H), 3.98 (dd, *J* = 8.9, 4.5 Hz, 4H), 3.75 (dd, *J* = 10.8, 6.1 Hz, 4H), 3.60 (s, 9H), 1.31 (d, *J* = 29.3 Hz, 10H), 1.05 (d, *J* = 6.5 Hz, 3H), 0.86 (t, *J* = 6.6 Hz, 3H). ^{13}C NMR (75 MHz, 298 K, $CDCl_3$) δ 156.19, 149.77, 145.87, 132.69, 115.25, 114.69, 108.97, 71.09, 71.00, 70.62, 70.45, 69.79, 69.54, 68.77, 46.29, 37.46, 31.94, 29.36, 26.22, 22.74, 21.60, 14.22. ESI-MS Calcd. for $C_{23}H_{39}N_2O_6$ (M + H^+) 439.3, Found 439.3; Calcd. for $C_{23}H_{38}N_2O_6Na$ (M + Na^+) 461.3, Found 461.3; Calcd for $C_{23}H_{38}N_2O_6K$ (M + K^+) 477.2, Found 477.3. HR-MS (ESI+) calcd. for $C_{23}H_{39}N_2O_6$ 439.2808 found *m*/*z* 439.2813

(S)-(Benzo-15-crown-5-15-yl)-3-(octan-2-yl)urea (**s2**), ^{1}H NMR (300 MHz, 298 K, DMSO-d_6) δ 8.09 (s, 1H), 7.14 (s, 1H), 6.81 (d, *J* = 8.7 Hz, 1H), 6.73 (d, *J* = 8.5 Hz, 1H), 5.84 (d, *J* = 8.1 Hz, 1H), 3.97 (s, 4H), 3.75 (s, 4H), 3.60 (s, 9H), 1.30 (d, *J* = 29.2 Hz, 10H), 1.05 (d, *J* = 6.5 Hz, 3H), 0.86 (t, *J* = 6.3 Hz, 3H). ^{13}C NMR (75 MHz, 298 K, $CDCl_3$) δ 156.09, 149.73, 145.63, 133.07, 115.34, 114.42, 108.74, 71.04, 70.94, 70.59, 70.41, 69.86, 69.78, 69.52, 68.74, 46.19, 37.49, 31.95, 29.38, 26.23, 22.74, 21.62, 14.22. ESI-MS Calcd. for $C_{23}H_{39}N_2O_6$ (M + H^+) 439.3, Found 439.4; Calcd. for $C_{23}H_{38}N_2O_6K$ (M + K^+) 477.2, Found 477.3. HR-MS (ESI+) calcd. for $C_{23}H_{39}N_2O_6$ 439.2808 found *m*/*z* 439.2810

1-(2-Ethylhexyl)-3-(benzo-15-crown-5-15-yl)urea (**3**), ^{1}H NMR (300 MHz, 298 K, DMSO-d_6) δ 8.18 (s, 1H), 7.13 (d, *J* = 2.1 Hz, 1H), 6.80 (d, *J* = 8.6 Hz, 1H), 6.74 (dd, *J* = 8.6, 2.1 Hz, 1H), 5.98 (t, *J* = 5.5 Hz, 1H), 4.07 – 3.93 (m, 4H), 3.74 (dd, *J* = 10.6, 5.9 Hz, 4H), 3.60 (s, 8H), 3.01 (d, *J* = 3.2 Hz, 2H), 1.40 – 1.13 (m, 9H), 0.86 (q, *J* = 7.0 Hz, 6H). ^{13}C NMR (75 MHz, 298 K, $CDCl_3$) δ 156.81, 149.72, 145.73, 132.87, 115.18, 114.47, 108.78, 71.06, 70.95, 70.61, 70.43, 69.78, 69.53, 68.72, 43.28, 39.77, 31.07, 29.00, 24.28, 23.18, 14.21, 10.99. ESI-MS Calcd. for $C_{23}H_{39}N_2O_6$ (M + H^+) 439.3, Found 439.3; Calcd for $C_{23}H_{38}N_2O_6Na$ (M + Na^+) 461.3, Found 461.3; Calcd. for $C_{23}H_{38}N_2O_6K$ (M + K^+) 477.2, Found 477.2. HR-MS (ESI+) calcd. for $C_{23}H_{39}N_2O_6$ 439.2808 found *m*/*z* 439.2809

2.4. Lipid Bilayer Transport Experiments

2.4.1. LUV Preparation for HPTS Experiments

The large unilamellar vesicles (LUVs) were formed using egg yolk L-α-phosphatidylcholine (EYPC chloroform solution, 800 μL, 20 mg). To this solution was added 800 μL of methanol MeOH and the solvent was slowly removed by evaporation under vacuum at room temperature and dried

overnight under high vacuum. The resulting thin film was hydrated with 400 μL of buffer (10 mM sodium phosphate, pH 6.4, 100 mM NaCl) containing 10 μM HPTS. During hydration, the suspension was submitted to seven freeze-thaw cycles (liquid nitrogen, water at room temperature). The obtained white suspension was extruded 21 times through a 0.1 μm polycarbonate membrane in order to transform the large multilamellar liposome suspension (LMVs) into LUVs with an average diameter of 100 nm. The LUVs suspension was separated from extra-vesicular HPTS dye by using size exclusion chromatography (SEC, stationary phase Sephadex G-50, mobile phase: phosphate buffer with 100 mM NaCl) and diluted with mobile phase to give 2.8 mL of 11mM lipid stock solution (considering all the lipids have been incorporated) [15].

2.4.2. Cation Transport Experiments

The fast filter method was used for data collection. 100 μL of stock vesicle solution was suspended in 1.85 mL of the corresponding buffer (10 mM PBS pH 6.4 containing 100 mM of the analyzed cation) and placed into a quartz fluorimetric cell. The emission of HPTS at 510 nm was monitored at two excitation wavelengths (403 and 460 nm) simultaneously. 0.464 mM lipid was used in each experiment. The final concentration of the compound is 0.06 mM for 12.9 mol% of compound/lipid ratio. This concentration is high enough for crown ethers to assemble as channels in lipid bilayers, assuming the insertion is complete. At 20 s, 29 μL of aqueous NaOH (0.5 M) was added, and macrocyclic compound added at 50 s, detergent was added after 340 s, and the measurement lasted another 50 s. For experiments involving FCCP, the compound was added at 40 s, and the tested macrocyclic compound was added at 60 s. The lysis started at 350 s for 50 s to finish the measurements this time. Experiments without FCCP (from 50 s to 340 s) are compared to experiments with FCCP (from 60 s to 350 s). The extent of transport was monitored using the ratio of the emission intensities of HPTS at 460 and 403 nm (I_{460} and I_{403}). We calculated the first-order initial rate constant from the slopes of the plot of ln ($[H^+]_{in} - [H^+]_{out}$) versus time, where $[H^+]_{in}$ and $[H^+]_{out}$ are the intravesicular and the extravesicular proton concentrations, respectively. The $[H^+]_{out}$ was assumed to remain constant during the experiment (pH 7.4), while $[H^+]_{in}$ values were calculated for each point from HPTS emission intensity using the equation $pH = 1.1684 \times \log(I_{460}/I_{403}) + 6.9807$. The initial and final pH are pH at $t = 0$ s and at the end of the experiment, respectively. In the picture, I refer to the intensity at 460 nm, and I_0 refers to intensity at 403 nm. To calculate EC_{50} and Hill coefficient n, we used the fractional activity Y. Y was calculated for each curve using the normalized value of I_{460}/I_{403} (just before lysis of the vesicles). We expressed Y as a function of time, and we performed fittings using a 2-parameter equation, which is, Hill equation: $Y = Y_{blank} + (Y_{max} - Y_{blank})/(1 + (EC_{50}/[C])^n)$, from which Y_{blank} is the fractional activity from the experiment of blank and Y_{max} is the largest fractional activity from the same series of experiments.

3. Results

Three octyl-benzoureido-15-crown-5-ethers have been prepared for the studies described here. The octyl-isocyanate (*R*)-(−)-2-octyl isocyanate, (*S*)-(+)-2-octyl isocyanate, 2-ethylhexyl isocyanate were treated with the corresponding 4-aminobenzo-15-crown-5-ether ($CHCl_3$, 65 °C, overnight) to afford after precipitation from hexane **1**, **r2**, **s2** and **3**, respectively, as powders (Scheme S1). ^{1}H-, ^{13}C-NMR, ESI-MS, and HR-MS spectroscopic data are in accord with proposed structures (see Supporting Information for details, Figures S1–S8).

The generation of functional transporting superstructures of **1**, **r2**, **s2** and **3** is based on three encoded features: (1) they contain macrocyclic cation-binding moieties [3–8]; (2) the supramolecular guiding interaction is the urea head-to-tail H-bond association, reminiscent with the amide H-bonding moiety in protein [9–15]; (3) the alkyl tails control the H-bonding self-assembly and induce variable hydrophobic stabilization at the interface with the bilayer membrane.

^{1}H NMR dilutions experiments on solutions in $CDCl_3$ of **1**, **r2**, **s2**, **3** show a variable downfield shift of both NH protons upon increasing the concentration, which is indicative of self-association through intermolecular H-bonding (Figure 2, Figures S9–S11). To quantify the degree of the aggregation, the NH shifts at different concentrations were fitted to the NMR CoEK aggregation

model (Nelder–Mead method) using Bindfit [9]. The determined values of the aggregation constants, as well as the cooperativity factors, are given in Table 1. There is encouraging strong cooperative H-bonding effect. The most associated compound **1** contains the linear *n*-octyl sidearm while the formation of aggregates is hindered when crowded supplementary residues block the H-bonding and slightly deactivate (~25% decrease) the self-association in **r2**, **s2** and **3**.

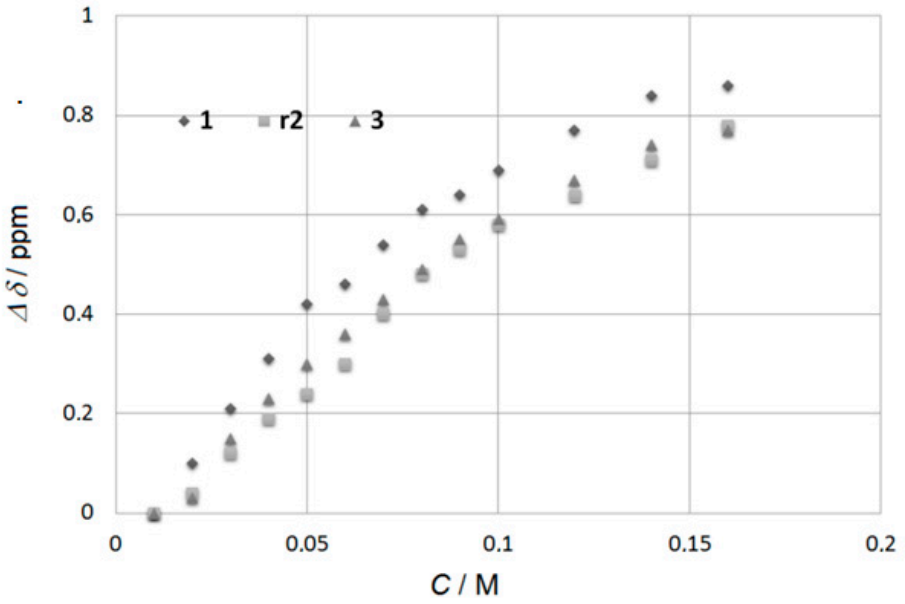

Figure 2. The difference in chemical shifts of the urea-type Ha protons relative to chemical shifts δ at 0.01 M plotted against the concentration of intermolecular H-bonded oligomers **1**, **r2**, and **3,** in $CDCl_3$ at 25 °C.

Table 1. Association Constants Ke for Numerical Fits a Monomer/Dimer/Aggregate model, obtained from NMR dilution experiments in $CDCl_3$ at 25 °C [9,13].

Compound	1	r2	3
K_e	19.3	15.3	14.6
ϱ [a]	0.23	0.10	0.20
K_e error (%)	2.64	3.89	2.30

[a] The factor $\varrho = K_d/K_e$ highlight the cooperativity of aggregation with $\varrho < 1$ positive cooperativity, $\varrho = 1$, no cooperativity and $\varrho > 1$ negative cooperativity for K_e aggregation vs. K_d dimerization.

The ion-transport activities were evaluated by the HPTS assay [24,25]. L-α-phosphatidylcholine, EYPC liposomes (Large Unilamellar Vesicles-LUV, 100 nm) were filled with a pH-sensitive dye, HPTS and 100 mM NaCl in a phosphate buffer (10 mM, pH 6.4). The liposomes were then suspended in an external phosphate buffer (10 mM, pH 6.4) containing 100 mM of MCl, $M^+ = Na^+, K^+$. Then, after addition of **1**, **r2**, **s2**, **3** in the bilayer membrane via injection of 20 μL of compound aliquots from stock 10 mM Dimethylsulfoxide (DMSO) solutions, see the final concentration values (% mol of the compound/mol of lipid) in hill plot analyses in Figure S12–S25), an external pH gradient was created by addition of NaOH. The internal pH change inside the liposome was monitored by the change in the fluorescence of HPTS (Figure 3a,b) [26].

Compounds **1**, **r2**, **s2,** and **3** are presenting subtle variations on the transport activities of monovalent K^+ and Na^+ cations, depending the structure of isomeric octyl substituents of ureido-benzo-15-crown-5 macrocycle. We note that enantiomers **s2** and **r2** have rather same activity for translocation of K^+ and Na^+ at the same concentration (Figure 3c). Under the same conditions, compounds **1**, **r2**, **s2** and **3** (12.9 mol%) present one order of magnitude higher initial transport rate

for K^+ cations than for Na^+, with kinetic selectivity of $S_{K+/Na+}$ = 3 to 6.6, depending on the compound (Tables S1 and S2 and Figure 4a).

Hill analysis [27] (Table 2, Figures S12–S25) revealed all macrocycles present K^+ over Na^+ selectivity, which is consistent with previous results. [8,15] Compound **1** is the most active, as it has the lowest EC_{50} for both Na^+ (10.6 mol%), and K^+ (4.1 mol%), much lower than its isomers following the transport activity sequence of **1** > **s2** > **3** within the μM concentration range. Compared with Valinomicin (EC_{50K+} = 5 pM) they are several orders of magnitude for K^+ activity. All the Hill coefficients are above 2, indicative of a formation of self-assembled aggregates containing more than two molecules of macrocycles, which transport cooperatively the cations, contrarily to Valinomycin acting as a carrier with a Hill number = 1 [27].

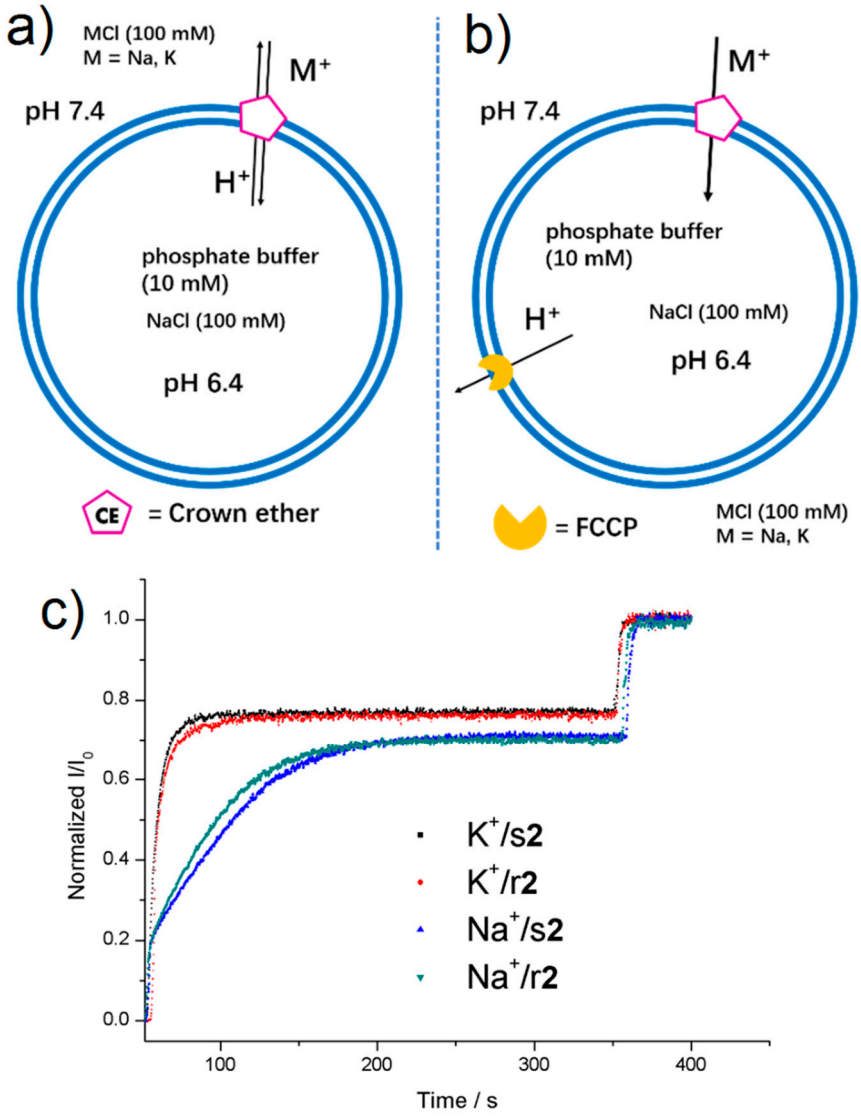

Figure 3. Schematic representation of the translocation mechanism in the presence of macrocycles (**a**) without or (**b**) with FCCP proton transporter. (**c**) Normalized I_{460}/I_{403} (I/I_0) versus time profiles for the transport of K^+ or Na^+ across the bilayer membrane promoted by **r2** or **s2** (32.3 mol%).

According to our previous results, the addition of alkyl-benzoureido-15-crown-5-ether channels in the membrane generate a quite stable transmembrane potential, following a $K^+ > H^+$ electrogenic antiport through the lipid bilayer [15]. We also know that the simultaneous addition of macrocycles and FCCP leads to the electrical coupling of fluxes and the transport can proceed without a potential across the membrane via a non-electrogenic exchange [28,29].

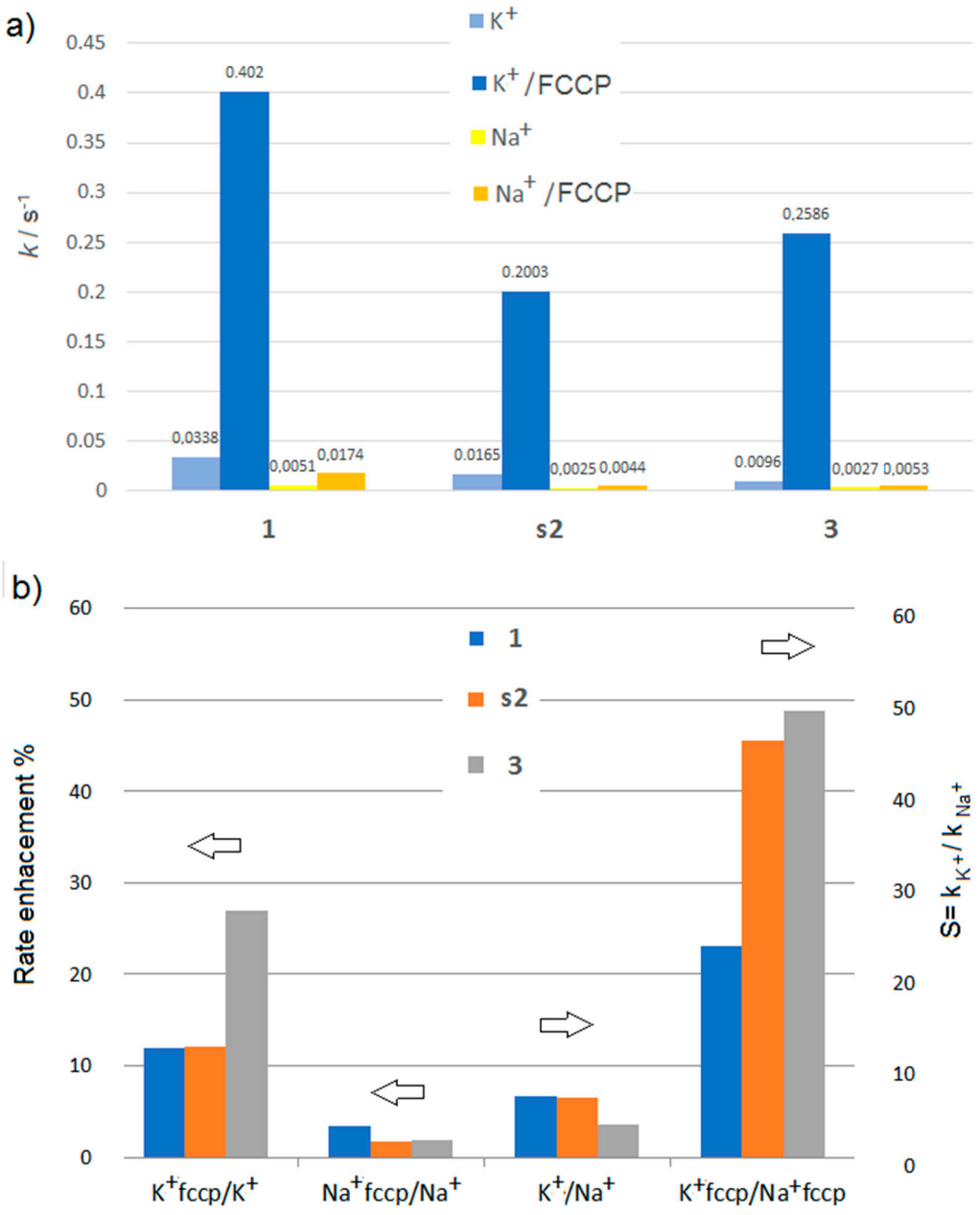

Figure 4. Bar graphs showing (**a**) the pseudo-first-order rate constants k (s^{-1}) for the transport of K^+ and Na^+ cations and (**b**) rate enhancement and K^+/Na^+ selectivity, for the macrocyclic carriers **1**, **s2**, **3**, (12.9 mol%) in presence or absence of protogenic FCCP carrier.

Table 2. Hill analysis results of K^+ and Na^+ transport with crown ethers **1**, **r2**, **s2**, **3**, in the presence or absence of FCCP. EC_{50} values expressed as mol% (% molar of compound/lipid needed to obtain 50% ion transport activity) and n is the Hill coefficient.

	K^+		K^+/FCCP		Na^+		Na^+/FCCP	
	EC_{50} [a] (mol%)	n [b]	EC_{50} [a] (mol%)	n	EC_{50} (mol%)	n	EC_{50} (mol%)	n
1	4.1	2.4	1.9	2.2	10.9	5.3	7.1	3.8
r2	/	/	3.0	3.2	/	/	10.7	4.1
s2	6.4	3.3	3.0	2.9	14.9	3.4	11.2	4.6
3	8.3	3.6	1.8	2.9	15.2	5.1	10.1	3.8

[a] EC_{50} was determined by the Hill plot, using the fractional activities at 340 s–290 s after the addition of the compound; [b] Hill coefficient.

As can be seen from Figure 4, the electrogenic component of the macrocyclic compound-mediated cation influx is stimulated by the addition of 0.1 mol% FCCP proton carrier as well, which overcome the proton transport rate-limiting barrier with a special emphasis for the transport of K^+ cations for which the transport rate show a 12 to 27 fold increase. This result is valid for all studied macrocycles **1**, **r2**, **s2**, **3**, for which the fractional activities Y for K^+ cations are also higher. This is also obvious from the EC_{50} values, which are strongly improving for K^+ but not for Na^+. FCCP improves transport efficiency, but more impressively, we observe an increase of S_{K^+/Na^+} selectivity from 6.6 to 45.5 in the case of **2** and from 3.6 to 48.8 in the case of **3**.

For all compounds, FCCP did improve transport activity towards Na^+, although not as much as K^+, and the rate of transport follows the sequence: $K^+ > Na^+ > H^+$. As far as we know, simple artificial systems presenting so high K^+/Na^+ selectivity are rare. It can be explained by several reasons: (i) The fact that these macrocycles can achieve this type of stable ionic potential, suited to drive protonic gradients, is simply due to their high selectivity for K^+. We know from our previous studies that similar compounds are selective for the transport of K^+ cations, even in the presence of Na^+ cations. [15] (ii) the formation of complexes is highly controlled via the formation of carrier dimers (benzo-15-crown-5-ether$_2K^+$) or higher oligomeric channels (benzo-15-crown-5-ether$_nK^+$). [13] Log *P* = 3.63−3.66 values, which are often used for evaluating the lipophilicity of the compound, are quite similar for all studied compounds **1**, **r2**, **s2**, **3**, thus, their partitions within the membrane might be similar (Table 3). Within this context, the branched alkyl chains might have a negative impact on the formation of the aggregates inside the lipid bilayer. Branched alkyl tails may favor the presence of low dimensional self-assembles species of **r2**, **s2,** or **3**. They show lower permeability than **1** (Figure 4a), but they lead to an increased S_{K^+/Na^+} selectivity via proton-mediated electrogenic conductance across the membrane (Figure 4b).

Table 3. Calculated logP (cLogP) values were obtained using VCC labs online calculator ALOGPS 2.1 to assess the lipophilicity of the compounds [30].

Compounds	logP
1	3.66
r2	3.64
s2	3.64
3	3.63

4. Conclusions

In conclusion, we demonstrated that macrocycles containing benzoureido-15-crown-5-ether cation-binding head and bearing linear or branched alkyl side-chains with almost identical lipophilicity, present completely different transport activities for translocations of cations across the lipid bilayer. The isomeric octyl-benzoureido-15-crown-5-ethers **1**, **r2**, **s2**, **3** described here, are very intriguing electrogenic macrocycles presenting K^+ over Na^+ kinetic selectivity of $S_{K+/Na+}$ = 3 to 6.6. Specifically, we have demonstrated that simple structural variation from linear to branched octyl chains are strongly influencing the transport activities of K^+ cations when compared with Na^+ cations. The electrogenic macrocyclic compound-mediated K^+ influx is highly increased up to 27 fold by the addition of FCCP proton carrier with a special emphasis for the transport of K^+ cations, for which the S_{K^+/Na^+} selectivity, is increasing from 6.6 to 45.5 in the case of **s2** and from 3.6 to 48.8 in the case of **3**. This is a significant step forward toward the development of electrogenic macrocycles with high K^+/Na^+ selectivity.

Supplementary Materials: The following are available online at www.mdpi.com/xxx/s1, Scheme S1: Synthesis of compounds **1**, **r,s2, 3**, Figure S1: ^{1}H NMR spectrum of **1** (300 MHz, 298K, DMSO-d6), Figure S2: ^{13}C NMR spectrum of **1** (75 MHz, 298K DMSO-d6), Figure S3 ^{1}H NMR spectrum of **r2** (300 MHz, 298 K, DMSO-d6), Figure S4 ^{13}C NMR spectrum of **r2** (75 MHz, 298 K, CDCl3), Figure S5 ^{1}H NMR spectrum of s**2** (300 MHz, 298 K, DMSO-d_6), Figure S6 ^{13}C NMR spectrum of s**2** (75 MHz, 298 K, $CDCl_3$), Figure S7 ^{1}H NMR spectrum of **3** (300 MHz, 298 K, DMSO-d_6), Figure S8 ^{13}C NMR spectrum of **3** (75 MHz, 298 K, $CDCl_3$), Figure S9 ^{1}H NMR dilution experiments

in $CDCl_3$ of **1** (0.01 to 0.16 M, from top to bottom), Figure S10 ^1H NMR dilution experiments in $CDCl_3$ of **r2** (0.01 to 0.16 M, from top to bottom), Figure S11 ^1H NMR dilution experiments in $CDCl_3$ of **3** (0.01 to 0.16 M, from top to bottom), Figure S12. Normalized I_{460}/I_{403} for transporting K^+ across the bilayer membrane facilitated by different amount of **1** and hill plot analysis of K^+/H^+ antiport, Figure S13. Normalized I_{460}/I_{403} for transporting Na^+ across the bilayer membrane facilitated by different amount of **1** and hill plot analysis of Na^+/H^+ antiport, Figure S14 Normalized I_{460}/I_{403} for transporting K^+ across the bilayer membrane facilitated by different amount of **1** coupled with FCCP (0.1 mol%) and hill plot analysis of K^+/H^+ antiport, Figure S15 Normalized I_{460}/I_{403} for transporting Na^+ across the bilayer membrane facilitated by different amount of **1** coupled with FCCP (0.1 mol%) and hill plot analysis of Na^+/H^+ antiport, Figure S16 Normalized I_{460}/I_{403} for transporting K^+ across the bilayer membrane facilitated by different amount of s**2** and Hill plot analysis of K^+/H^+ antiport, Figure S17 Normalized I_{460}/I_{403} for transporting Na^+ across the bilayer membrane facilitated by different amount of s**2** and hill plot analysis of Na^+/H^+ antiport, Figure S18 Normalized I_{460}/I_{403} for transporting K^+ across the bilayer membrane facilitated by different amount of s**2** coupled with FCCP (0.1 mol%) and hill plot analysis of K^+/H^+ antiport, Figure S19 Normalized I_{460}/I_{403} for transporting Na^+ across the bilayer membrane facilitated by different amount of s**2** coupled with FCCP (0.1 mol%) and hill plot analysis of Na^+/H^+ antiport, Figure S20 Normalized I_{460}/I_{403} for transporting K^+ across the bilayer membrane facilitated by different amount of r**2** coupled with FCCP (0.1 mol%) and hill plot analysis of K^+/H^+ antiport, Figure S21 Normalized I_{460}/I_{403} for transporting Na^+ across the bilayer membrane facilitated by different amount of r**2** coupled with FCCP (0.1 mol%) and hill plot analysis of Na^+/H^+ antiport, Figure S22 Normalized I_{460}/I_{403} for transporting K^+ across the bilayer membrane facilitated by different amount of **3** and hill plot analysis of K^+/H^+ antiport, Figure S23 Normalized I_{460}/I_{403} for transporting Na^+ across the bilayer membrane facilitated by different amount of **3** and hill plot analysis of Na^+/H^+ antiport, Figure S24 Normalized I_{460}/I_{403} for transporting K^+ across the bilayer membrane facilitated by different amount of **3** coupled with FCCP (0.1 mol%) and hill plot analysis of K^+/H^+ antiport, Figure S25 Normalized I_{460}/I_{403} for transporting Na^+ across the bilayer membrane facilitated by different amount of **3** coupled with FCCP (0.1 mol%) and hill plot analysis of Na^+/H^+ antiport, Figure S26. HR-MS spectra of compounds **1, r2, s2, 3,** Table S1 Pseudo first-order rate constants k (s^{-1}) for the transport of K^+/H^+ through LUVs at different concentrations of the compounds to lipid without or with proton transporter FCCP, Table S2 Pseudo first-order rate constants k (s^{-1}) for the transport of Na^+/H^+ through LUVs at different concentrations of the compounds to lipid without or with proton transporter FCCP. The initial rate for the blank has already been subtracted from all the rates.

Author Contributions: **C**onceptualization—M.B. Synthesis, Cation Transport—Y.-H.L. and S.-P.Z.; Investigation—D.W.; Writing—Original Draft Preparation—Y.-H.L. and M.B.; Supervision—M.B.; Funding Acquisition—M.B. All authors have read and agreed to the published version of the manuscript.

Funding: This work was also conducted within ANR-18-CE06-0004-02, WATERCHANNELS, and 1000 Talent Plan, WQ20144400255 of SAFEA, China. Y-H. L. wishes to thank the Innovation and Talent Introduction Base of Photoelectronic and Functional Molecular Solids Material (Grant No. 90002-18011002) from Sun Yat-Sen University, and also the China Scholarship Council (No. 201606380054) for the financial support. NSFC (National Natural Science Foundation of China, 21720102007), China. S.-P.Z. wishes to thank the China Scholarship Council for financial support.

Conflicts of Interest: The authors declare no conflict of interest. The funders had no role in the design of the study; in the collection, analyses, or interpretation of data; in the writing of the manuscript, or in the decision to publish the results.

References

1. Hille, B. *Ion Channels of Excitable Membranes*, 3rd ed.; Sinauer Associates: Sunderland, MA, USA, 2001.
2. Sakai, N.; Gerard, D.; Matile, S. Electrostatics of Cell Membrane Recognition: Structure and Activity of Neutral and Cationic Rigid Push-Pull Rods in Isoelectric, Anionic, and Polarized Lipid Bilayer Membranes *J. Am. Chem. Soc.* **2001**, *123*, 2517–2524.
3. Barboiu, M. Supramolecular Polymeric Macrocyclic Receptors—Hybrid Carrier vs. Channel Transporters in Bulk Liquid Membranes. *J. Incl. Phenom. Macrocycl. Chem.* **2004**, *49*, 133–137.
4. Otis, F.; Racine-Berthiaume, C.; Voyer, N. How Far Can a Sodium Ion Travel within a Lipid Bilayer? *J. Am. Chem. Soc.* **2011**, *133*, 6481–6483.
5. Otis, F.; Auger, M.; Voyer, N. Exploiting Peptide Nanostructures to Construct Functional Artificial Ion Channels. *Acc. Chem. Res.* **2013**, *46*, 2934–2943.
6. Weber, M.E.; Schlesinger, P.H.; Gokel, G.W. Dynamic Assessment of Bilayer Thickness by Varying Phospholipid and Hydraphile Synthetic Channel Chain Lengths. *J. Am. Chem. Soc.* **2005**, *127*, 636–642.

7. Gokel, G.W.; Negin, S. Synthetic membrane active amphiphiles. *Adv. Drug Deliv. Rev.* **2012**, *64*, 784–796.
8. Ren, C.; Shen, J.; Zeng, H. Combinatorial Evolution of Fast-Conducting Highly Selective K^+-Channels via Modularly Tunable Directional Assembly of Crown Ethers. *J. Am. Chem. Soc.* **2017**, *139*, 12338–12341.
9. Webb, J.E.A.; Crossley, M.J.; Turner, P.; Thordarson, P. Pyromellitamide Aggregates and Their Response to Anion Stimuli. *J. Am. Chem. Soc*. **2007**, *129*, 7155–7162.
10. Zheng, S.P.; Li, Y.H.; Jiang, J.J.; van der Lee, A.; Dumitrescu, D.; Barboiu, M. Self-Assembled Columnar Triazole-Quartets—An example of synergetic H-bonding/Anion-π Channels. *Angew. Chem. Int. Ed.* **2019**, *58*, 12037–12042.
11. Barboiu, M.; Cerneaux, S.; Van der Lee, A.; Vaughan, G. Ion-driven ATP-pump by Self-Organized Hybrid Membrane Materials. *J. Am. Chem. Soc.* **2004**, *126*, 3545–3550.
12. Mihai, S.; Cazacu, A.; Arnal-Herault, C.; Nasr, G.; Meffre, A.; van der Lee, A.; Barboiu, M. Supramolecular self-organization in constitutional hybrid materials. *New J. Chem.* **2009**, *33*, 2335–2343.
13. Cazacu, A.; Tong, C.; van der Lee, A.; Fyles, T.M.; Barboiu, M. Columnar Self-Assembled Ureidocrown-ethers—An Example of Ion-channel Organization in Lipid Bilayers. *J. Am. Chem. Soc.* **2006**, *128*, 9541–9548.
14. Cazacu, A.; Legrand, Y.M.; Pasc, A.; Nasr, G.; Van der Lee, A.; Mahon, E.; Barboiu, M. Dynamic hybrid materials for constitutional selective membranes. *Proc. Natl. Acad. Sci. USA* **2009**, *106*, 8117–8122.
15. Gilles, A.; Barboiu, M. Highly Selective Artificial K^+ Channels: An Example of Selectivity- Induced Transmembrane Potential. *J. Am. Chem. Soc.* **2016**, *138*, 426–432.
16. Sun, Z.; Barboiu, M.; Legrand, Y.M.; Petit, E.; Rotaru, A. Selective Artificial Cholesteryl Crown Ether K^+-Channels. *Angew. Chem. Int. Ed.* **2015**, *54*, 14473–14477.
17. Sun, Z.; Gilles, A.; Kocsis, I.; Legrand, Y.M.; Petit, E.; Barboiu, M. Squalene Crown-Ether Self-assembled Conjugates—An example of highly selective artificial K^+-channels. *Chem. Eur. J.* **2016**, *22*, 2158–2164.
18. Feng, W.X.; Sun, Z.; Zhang, Y.; Legrand, Y.M.; Petit, E.; Su, C.Y.; Barboiu, M. Bis-15-Crown-5-Ether-Pillar[5]arene K^+-Responsive Channels. *Org. Lett.* **2017**, *19*, 1438–1141.
19. Schneider, S.; Licsandru, E.D.; Kocsis, I.; Gilles, A.; Dumitru, F.; Moulin, E.; Tan, J.J.; Lehn, J.M.; Giuseppone, N.; Barboiu, M. Columnar Self-Assemblies of Triarylamines as Scaffolds for Artificial Biomimetic Channels for Ion and for Water Transport. *J. Am. Chem. Soc.* **2017**, *139*, 3721–3727.
20. Spooner, M.J.; Gale, P.A. Anion transport across varying lipid membranes—The effect of lipophilicity. *Chem. Commun.* **2015**, *51*, 4883–4886.
21. Knight, N.J.; Hernando, E.; Haynes, C.J.E.; Busschaert, N.; Clarke, H.J.; Takimoto, K.; Garcia-Valverde, M.; Frey, J.G.; Quesada, R.; Gale, P.A. QSAR analysis of substituent effects on tambjamine anion transporters. *Chem. Sci.* **2016**, *7*, 1600–1608.
22. Saggiomo, V.; Otto, S.; Marques, I.; Felix, V.; Torroba, T.; Quesada, R. The role of lipophilicity in transmembrane anion transport. *Chem. Commun.* **2012**, *48*, 5274–5276.
23. Li, Z.; Deng, L.Q.; Chen, J.X.; Zhou, C.Q.; Chen, W.H. Does lipophilicity affect the effectiveness of a transmembrane anion transporter? Insight from squaramido-functionalized bis(choloyl) conjugates. *Org. Biomol. Chem.* **2015**, *13*, 11761–11769.
24. Berezin, S.K.; Davis, J.T. Catechols as Membrane Anion Transporters. *J. Am. Chem. Soc.* **2009**, *131*, 2458–2459.
25. Li, Y.H.; Zheng, S.P.; Legrand, Y.M.; Gilles, A.; Van der Lee, A.; Barboiu, M. Structure-driven selection of adaptive transmembrane Na^+ carriers or K^+ channels. *Angew. Chem. Int. Ed.* **2018**, *57*, 10520–10524.
26. Matile, S.; Sakai, N. *Analytical Methods in Supramolecular Chemistry*; Schalley, C.A., Ed.; Wiley-VCH: Weinheim, Germany, 2007; pp. 381–418.
27. Bhosale, S.; Matile, S. A Simple Method to Identify Supramolecules in Action: Hill Coefficients for Exergonic Self-Assembly. *Chirality* **2006**, *18*, 849–856.
28. Valkenier, H.; Haynes, C.J.E.; Herniman, J.; Gale, P.A.; Davis, A.P. Lipophilic balance—A new design principle for transmembrane anion carriers. *Chem. Sci.* **2014**, *5*, 1128–1134.

29. Wu, X.; Judd, L.W.; Howe, E.N.W.; Withecombe, A.M.; Soto-Cerrato, V.; Li, H.; Busschaert, N.; Valkenier, H.; Pérez-Tomás, R.; Sheppard, D.N.; et al. Nonprotonophoric Electrogenic Cl^- Transport Mediated by Valinomycin-like Carriers. *Chem* **2016**, *1*, 127–146.
30. Varnek, A.; Gaudin, C.; Marcou, G.; Baskin, I.; Pandey, A.K.; Tetko, I.V. Inductive Transfer of Knowledge: Application of Multi-Task Learning and Feature Net Approaches to Model Tissue-Air Partition Coefficients. *J. Chem. Inf. Model.* **2009**, *49*, 133–144.